Environmental Science & Technology Letters

pubs.acs.org/journal/estlcu

Letter

Open Access

This article is licensed under CC-BY-NC-ND 4.0

Amino Acid Complexation Fractionates Nickel Isotopes: Implications for Tracing Nickel Cycling in the Environment

Corday R. Selden,* Kathrin Schilling, Anirban Basu, Jennifer Timm, Naomi Saunders, and Nathan Yee

Cite This: *Environ. Sci. Technol. Lett.* 2025, 12, 283−288

Read Online

ACCESS | Metrics & More | Article Recommendations | Supporting Information

ABSTRACT: Nickel (Ni) is an essential cofactor in many proteins. Ni stable isotopes have been shown to undergo isotope fractionation in microorganisms and plants. However, the mechanisms driving this fractionation are poorly understood. Here, we present experimental data on Ni isotope fractionation during binding by common Ni-binding amino acids: glutamate (carboxylate side chain), histidine (imidazole side chain), and cysteine (sulfhydryl side chain). We used an equilibrium Donnan dialysis approach to separate free versus bound Ni and measured the isotopic composition of both pools via multicollector inductively coupled plasma mass spectrometry (MC-ICP-MS). Our results reveal that the glutamate and cysteine favor heavy ^{60}Ni ($\Delta^{60/58}Ni_{glutamate}$ = +0.80 ± 0.08; $\Delta^{60/58}Ni_{cysteine}$ = +1.27 ± 0.08‰), while histidine causes little isotope shift (−0.12 ± 0.16‰). We then conducted experiments using a short peptide that is a structural analogue for acetyl-CoA synthetase and Ni-iron hydrogenase metal-binding sites. The peptide preferentially bound the heavy ^{60}Ni with a $\Delta^{60/58}Ni_{peptide}$ value of +0.74 ± 0.04‰. The Ni isotope effect associated with peptide binding corresponded directly to the fractionation expected based on the coordinating ligands. This work represents an important first step in understanding the mechanistic controls on Ni isotope fractionation and the drivers of Ni isotope fractionation in biological and environmental systems.

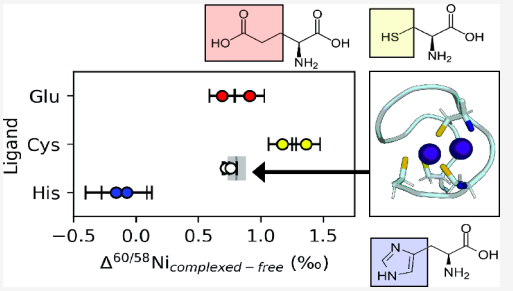

KEYWORDS: *nickel, isotope, protein, biosignature, biomolecule, thiol, dialysis, mechanism*

INTRODUCTION

Nickel (Ni) stable isotope analysis is an emerging tool for investigating biological Ni cycling in the environment.[1] Nickel isotope fractionation has been observed in a wide range of biological systems, including plants,[2−5] phytoplankton,[6−8] and methanogenic archaea.[9] In plants, Ni isotopes are fractionated in roots and leaves, highlighting their utility to track physiological pathways including uptake, translocation, and metal storage.[2−5] Similarly, diverse phytoplankton differentially fractionate Ni isotopes, with implications for understanding microbial metabolism in the ocean.[6,7,10,11] Finally, it has been observed that Ni in methanogenic archaea is isotopically distinct from nonmethanogens, suggesting that Ni isotopes could serve as a biosignature.[9] However, the direction of these fractionations varies across biological systems and with physiological states, complicating their interpretation.

Complexation to organics is a key process controlling Ni cycling and isotope fractionation.[12,13] Amino acids are the most important types of organic ligands that bind Ni in biological systems. In the Protein Data Bank, the world's repository of experimentally resolved protein structures, the most common amino acids that bind Ni are aspartic and glutamic acid, cysteine, and histidine.[14] These amino acids coordinate metals using oxygen (O), sulfur (S), and nitrogen (N) atoms in their carboxyl, sulfhydryl, and imidazole functional groups, respectively. Currently, the direction and magnitude of Ni isotope fractionation by amino acid complexation have not been quantified.

The goal of this study was to experimentally determine Ni isotope fractionation due to ligation by glutamate, histidine, and cysteine. We also investigated Ni isotope fractionation by a higher-order structure: a 13 amino acid-long peptide that coordinates two Ni atoms using four S and two N residues.[15] These sites are, respectively, structural analogs for Ni-binding sites in acetyl-CoA synthase and Ni-iron (Fe) hydrogenase (NiFe-H_2ase),[15] two ancient enzymes that mediate core biogeochemical processes. This work provides the first quantitative evidence that common metal-binding amino acids differentially fractionate Ni and that these signatures are consistent at higher levels of biological complexity.

METHODS AND MATERIALS

Amino Acid−Ni Ligation Experiments. Ni−amino acid complexation experiments were conducted in an electrolyte solution containing 10 mM strontium nitrate (>99.995%

Received: December 6, 2024
Revised: January 8, 2025
Accepted: January 9, 2025
Published: February 27, 2025

© 2025 The Authors. Published by American Chemical Society

purity, Sigma-Aldrich) and 5 mM HEPES (4-(2-hydroxyethyl)piperazine-1-ethane-sulfonic acid) buffer (>99.5%, Sigma-Aldrich; Table S1). 100 μM of Ni^{2+} (100 μM, Sigma-Aldrich, Ni nitrate standard) was reacted with 200 μM glutamate, cysteine, or histidine. Glutamate and cysteine (Sigma-Aldrich) were reagent-grade (>95%); histidine was a higher purity (BioUltra, >99.5%). To avoid disulfide bridging, Ni−cysteine complexation was carried out under anoxic conditions in acid-washed (2 days in 20% nitric acid) glass serum vials with a N_2 headspace. Ni−glutamate and Ni−histidine complexation was carried out in air in acid-washed centrifuge tubes (LabCon). For all complexation experiments, the Ni−amino acid solutions were adjusted to pH 8.2 with sodium hydroxide and then allowed to react overnight (~16 h) at room temperature; as Ni−amino acid complexes form within seconds,[16,17] this duration allowed ample time for complete equilibration. All reagents were prepared using ultrapure deionized water (18.2 MΩ·cm, Milli-Q, Millipore).

At the end of each complexation experiment, free Ni^{2+} and ligated Ni were separated using an equilibrium Donnan dialysis approach.[18,19] In brief, the Ni−amino acid solution (i.e., donor) is placed in one chamber of a clean (2 days in 20% nitric acid (HNO_3) PTFE microequilibrium dialyzer (Harvard Apparatus 7416-15001D; 1.5 mL cells) and dialyzed against a background electrolyte solution (i.e., acceptor) using a strong-acid cation-exchange membrane (Nafion-117, E.I. Dupont de Nemours). The cation-exchange membrane permits the passage of free Ni^{2+}, but not bound Ni. Free Ni^{2+} thus equilibrates across the membrane and accumulates in the acceptor solution, while ligated Ni is retained in the donor solution. Prior to the experiment, the cation-exchange membrane was washed in ultrapure water (3 successive soaks, 2+ days) and preconditioned with acceptor solution.

Once placed in the dialyzer, the solutions were equilibrated across the cation-exchange membrane for 27 h. No-ligand control experiments indicated that dialysis reached mass and isotopic equilibrium within 1 day (Figure S1; Table S2; Suppl. Text 1). Samples were collected before (t = 0) and after (t = final) dialysis for mass and isotope analysis. Ni concentrations were measured in all solutions via inductively coupled plasma optical emissions spectroscopy (ICP-OES; iCAP 7400, ThermoFisher), with an average detection limit (3σ, n > 5 blanks) of 0.30 μM of Ni. We note that some Ni is lost from the solution due to membrane adsorption;[20] this adsorption is likely reversible and does not fractionate Ni (see Suppl. Text 1).

Peptide−Ni Ligation Experiments. The custom apopeptide (amino acid sequence: CNCGCGNNNDRCG) was purchased as a lyophilized powder from Genscript Biotech (Piscataway, NJ) and stored frozen (−80 °C). Peptide reconstitution occurred overnight under anoxic conditions, as described previously.[15] The reconstitution matrix contained 100 mM sodium chloride (>99%, Sigma-Aldrich), 25 mM HEPES, 3.75 mM freshly prepared TCEP (tris-2-carboxyethyl-phosphine hydrochloride), and 600 μM Ni ($NiCl_2$, Sigma-Aldrich) and was adjusted to pH 7.5 using trace sodium hydroxide and hydrochloric acid (HCl). At the end of the complexation experiment, the di-Ni cluster assembly was verified using circular dichroism (CD) spectroscopy (AVIV420, 50 °C). We also conducted CD spectral analysis of the Ni−peptide after dialysis to ensure that the complex did not morph during dialysis. A nonligand control (the anoxic reconstitution solution) was prepared in parallel.

The dialysis system was prepared as described above; the final membrane pretreatment step and sample dialysis were carried out in an anoxic chamber (95% N_2, 5% H_2). Due to the higher ionic strength of the matrix, the system was slower to equilibrate, approaching equilibrium ~40 h during preliminary trials (Figure S1B). To ensure complete equilibration in experiments, peptide trials were ended at 66 h; equilibration was confirmed in a parallel no-ligand control experiment (Table S2). Ni concentrations were determined by ICP-OES as described above.

Ni Purification and Isotope Analysis. Ni isotopes were analyzed in all experimental solutions (Table S3). Ni was purified using a method modified from Gall et al.[21] with only one column chemistry purification step (see Suppl. Text 2 for rationale). An 1100 ng Ni aliquot of each sample was transferred to a Savillex PFA vial and weighed on a 5-figure balance, dried (120 °C), and resuspended in 7.8 M HNO_3. To correct for any isotopic fractionation during sample purification and mass spectrometry, a double spike (25:75 ^{61}Ni:^{62}Ni) was added and weighed for a total Ni mass per sample of 3850 ng. Spiked samples were refluxed at 85 °C until equilibrated, dried again, dissolved in 6 M HCl, and resuspended for a final concentration of 0.1 M HCl and 0.05 M oxalic acid. Microcolumns (PTFE; 250 μL column with 1.5 mL reservoir) were prepared by loading with AG50W-X4 resin (200−400 mesh) and alternately rinsed with 6 M hydrochloric acid and ultrapure water (3×), followed by a final equilibration in a solution of 0.05 M oxalic acid and 0.1 M HCl solution. Samples were loaded onto columns and then rinsed with the 0.1 M HCl/0.05 M oxalic acid mix (3×, 1 mL), followed by 0.5 M HCl in 95% acetone (3×, 1 mL). These rinses remove s-block elements, including sodium. Finally, Ni was eluted with 1 mL of a freshly prepared solution (95% acetone, 0.1 M dimethylglyoxime [DMG], and 0.05 HCl) into a clean Teflon beaker containing 150 μL of ultrapure water to prevent volatilization. Samples were dried at 90 °C for ~1.5 h. The Ni−DMG complex remaining was acidified with 100 μL concentrated HNO_3 and dried. Another 100 μL of concentrated HNO_3 was added, and samples were finally refluxed overnight at 150 °C and then dried again. Samples were dissolved in 50% concentrated HNO_3 and diluted with ultrapure water for a 2% HNO_3 analysis matrix.

Ni isotope ratios were measured on a Nu Plasma Sapphire multicollector inductively coupled plasma mass spectrometer in high resolution mode (MC-ICP-MS; Columbia University) with standard bracketing at 350.[22,23] The double spike was deconvoluted online.[24] Data were normalized to NIST isotopic standard SRM986 as

$$\delta^{60}\mathrm{Ni}(‰) = \left[\frac{\frac{^{60}\mathrm{Ni}}{^{58}\mathrm{Ni}_{\mathrm{sample}}}}{\frac{^{60}\mathrm{Ni}}{^{58}\mathrm{Ni}_{\mathrm{SRM986}}}} - 1\right] \times 1000 \quad (1)$$

To assess instrument accuracy and ensure that sample preparation did not fractionate Ni, we ran two in-house standards with and without column chemistry. Our measurements are within error of published[23] values and standards run through columns were isotopically indistinguishable from no-chemistry standards (Table S4).

Ni Mass Balance. The δ^{60}Ni value of complexed Ni was calculated by using a mass balance equation with the free Ni^{2+}

https://doi.org/10.1021/acs.estlett.4c01060
Environ. Sci. Technol. Lett. 2025, 12, 283−288

pool, the δ^{60}Ni of which was measured directly in the acceptor solution:

$$\delta^{60}\mathrm{Ni}_{\mathrm{complexed}} = \frac{\delta^{60}\mathrm{Ni}_{\mathrm{total}} - (\delta^{60}\mathrm{Ni}_{\mathrm{acceptor}} \times f_{\mathrm{free}})}{(1 - f_{\mathrm{free}})} \quad (2)$$

Here, f_{free} indicates the relative proportion of free Ni^{2+} at t = final, calculated as

$$f_{\mathrm{free}} = \frac{2 \times \mathrm{mass}_{\mathrm{acceptor}}}{(\mathrm{mass}_{\mathrm{donor}} + \mathrm{mass}_{\mathrm{acceptor}})} \quad (3)$$

where "mass$_x$" indicates the total Ni mass measured in the acceptor or donor chamber. Since free Ni^{2+} equilibrates across the membrane, two times the acceptor chamber mass represents the total mass of free Ni^{2+} in the system. We calculated the relative isotope abundance of all dissolved Ni ($\delta^{60}\mathrm{Ni}_{\mathrm{total}}$) at t = final as

$$\delta^{60}\mathrm{Ni}_{\mathrm{total}} = \delta^{60}\mathrm{Ni}_{\mathrm{acceptor}} \times f_{\mathrm{acceptor}} + \delta^{60}\mathrm{Ni}_{\mathrm{donor}} \times f_{\mathrm{donor}} \quad (4)$$

where f indicates the fractional contribution at t = final of the acceptor and donor chambers to the total Ni pool:

$$f_{\mathrm{donor}} = \frac{\mathrm{mass}_{\mathrm{donor}}}{(\mathrm{mass}_{\mathrm{donor}} + \mathrm{mass}_{\mathrm{acceptor}})} \quad (5)$$

Finally, Ni isotope separation values between complexed and free Ni^{2+} were calculated as follows:

$$\Delta\mathrm{Ni}_{\mathrm{complexed\text{-}free}} = \delta^{60}\mathrm{Ni}_{\mathrm{complexed}} - \delta^{60}\mathrm{Ni}_{\mathrm{free}} \quad (6)$$

All error reported for isotope measurements is propagated from the 2SD of multiple analytical replicates (Table S3).

RESULTS AND DISCUSSION

Ni Isotope Fractionation during Complexation by Amino Acids. Ni-binding by amino acid ligands was observed in all experiments, as demonstrated by the greater retention of Ni in the donor chamber of the dialyzer, which contained both the Ni-ligand complexes and free Ni^{2+}, compared to that in the acceptor solutions, which contained only Ni^{2+}, following dialysis. In duplicate experiments, Ni retention was greater for cysteine trials (87.5% and 83.3%) than in glutamate (70.0% and 71.2%) or histidine (63.2% and 66.8%) trials, indicating a larger proportion of bound Ni. Assuming full free Ni^{2+} equilibration across the two chambers, an average of 70.8, 41.2, and 30.0% Ni was bound to cysteine, glutamate, and histidine, respectively (Table S3).

Glutamate and cysteine favored heavy ^{60}Ni, while histidine showed little isotope effect (Table S6; Figure 1). The calculated fractionation ($\Delta^{60}\mathrm{Ni}_{\mathrm{complex\text{-}free}}$) was greatest for cysteine (+1.27 ± 0.08‰), moderate for glutamate (+0.80 ± 0.08‰), and negligible for histidine (−0.12 ± 0.16‰) (Table S6; Figure 1). Independent duplicate trials were all in good agreement (Table S3).

While there are no theoretical predictions available in the literature that offer direct comparison, reduced partition functions (lnβ) derived from Density Functional Theory are available for several carboxylates and carbonates, which are in good agreement with our experimental observation for glutamate.[25,26] Differences between lnβ values of different chemical species are analogous to isotope separation values ($\Delta_{\mathrm{A\text{-}B}}$). Nickel carbonate ($NiCO_3(H_2O)_4$), for example, has a

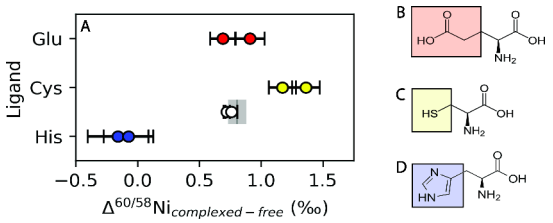

Figure 1. Isotope separation values (A; $\Delta^{60}\mathrm{Ni}_{\mathrm{complexed\text{-}free}} = \delta^{60}\mathrm{Ni}_{\mathrm{complex}} - \delta^{60}\mathrm{Ni}_{\mathrm{free}}$) and structures for the amino acids: glutamic acid (B, red), cysteine (C, yellow), and histidine (D, blue). Points represent independent experiments; bars represent propagated analytical uncertainty (2SD); boxes in plots B–D highlight the side chain. The gray bar denotes fractionation of the peptide predicted from histidine and cysteine data; the shaded gray area indicates propagated uncertainty. White points show measured experimentally derived peptide values.

lnβ that is +0.557‰ greater than that of free Ni ($Ni(H_2O)_6^{2+}$) in an aqueous solution at 298 K.[25] Nickel oxalate (NiC_2O_4)[25] and citrate ($NiH_2(cit)(H_2O)_3^+$),[26] similarly, are +0.917‰ and +0.436‰ greater than free Ni. These values are in the same range and direction as for our glutamate experiments (+0.80 ± 0.08‰). Moreover, they are consistent with the behavior of other bioactive transition metal isotope systems (e.g., copper) in experimental[18,19] and computational studies.[26] Interestingly, work with natural carboxyl ligands suggests a negligible isotope effect, <+0.2‰.[5] This difference in magnitude may reflect experimental conditions (e.g., pH, stoichiometry of experimental solutions, and resultant chemical speciation of the metal).

There are few direct points of comparison at the molecular level for Ni-binding by molecules comparable to those of cysteine or histidine. For histidine, our results are consistent with observations from comparable metal isotope systems, such as zinc and copper. For zinc, histidine-binding is predicted to impart a negligible isotope effect, ranging from −0.267 to 0.106‰ depending on coordination geometry and hydration state.[26] Experimental[19] and theoretical[26] works for copper show similarly small effects. Interestingly, in copper and zinc isotope biochemistry, cysteine binding generally favors the light isotope.[19,26]

Scaling Ni Isotope Fractionation from Amino Acids to Proteins. The dinuclear Ni peptide (Figure 2A) used in our

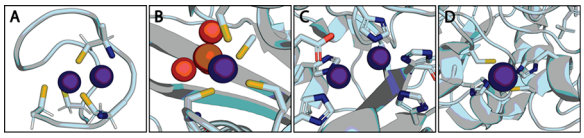

Figure 2. Ni-binding sites in (A) the experimental peptide,[15] (B) Ni-iron hydrogenase (NiFe-H_2ase; PDB ID: 1FRV), (C) urease (PDB ID: 4CEU), and (D) urease assembly protein UreG in apo form (PDB ID: 5XKT). Ni, N, S, and O are colored purple, blue, yellow, and red, respectively. In panel B, a hydrated iron atom appears in orange.

experiments was designed by Timm and colleagues[15] as a structural analog for metal-binding sites in two ancient enzymes: acetyl-CoA synthetase, involved in acetate metabolism, and NiFe-H_2ase (Figure 2B), which interconverts molecular hydrogen and protons in many prokaryotes. It binds two Ni atoms using a combination of four thiols from cysteine and two amides (N groups) in its backbone.

https://doi.org/10.1021/acs.estlett.4c01060
Environ. Sci. Technol. Lett. 2025, 12, 283−288

As in our amino acid trials, ligand-Ni binding was evidenced in peptide trials by retention of Ni in the dialyzer chamber containing the peptide (76.1% and 76.0% in two respective trials). From this, we calculate that an average of 52.8% of Ni was peptide-bound (Table S3).

The peptide preferentially bound heavy ^{60}Ni. This is clearly shown in the $\delta^{60}Ni_{complex}$ values calculated for each trial (+0.60 ± 0.02‰ and +0.60 ± 0.04‰, respectively) relative to those measured in the free Ni^{2+} pool (−0.12 ± 0.01‰ and +0.16 ± 0.02‰; Table S5). From these values, we calculate $\Delta^{60}Ni_{complex\text{-}free}$ values of +0.72 ± 0.03‰ and +0.76 ± 0.05‰ for the two experimental trials (Tables S4 and S5).

This isotope fractionation was highly consistent with that predicted from our trials with N and S ligands, despite differences in the experimental conditions (e.g., pH and ionic strength). We performed preliminary calculations to predict the $\Delta^{60}Ni_{peptide\text{-}free}$ from trials with histidine and cysteine: Taking the average $\Delta^{60}Ni_{His\text{-}free}$ and $\Delta^{60}Ni_{Cys\text{-}free}$ values (Table S5) and weighting based on the binding site stoichiometry of the peptide (4S:2N:2Ni), we estimate a $\Delta^{60}Ni_{peptide\text{-}free}$ of +0.81 ± 0.07‰. This value is remarkably close to the measured mean of +0.74 ± 0.03‰. Though more observations are necessary to reach statistical significance, this astounding parity suggests that the identity and stoichiometry of the ligands that directly coordinate Ni represent the greatest source of variability in the protein-level isotope effect; further experiments are necessary to unravel the relative impact of other factors (e.g., folding environment and outer sphere molecular interactions).

Environmental Relevance. Our experiments indicate that Ni complexation to thiols such as cysteine can impart large Ni isotope fractionation ($\Delta^{60}Ni_{Cys}$ = +1.27 ± 0.08‰). Typically occurring in excess of metal concentrations, thiols are important metal-binding ligands in a wide range of aquatic environments.[27−31] Voltametric measurements indicate that 10−50% of dissolved Ni is bound to strong organic ligands.[32−34] Thiols form strong and stable complexes,[35] particularly in the dissolved rather than particulate phase.[27,29] In surface waters, where there is no redox-driven Ni isotope fractionation,[36] the particulate pool can be <0.5‰ lighter than the dissolved Ni pool.[6,36,37] Indeed, the dissolved pool of Ni has been found to be isotopically heavy across diverse aquatic regimes.[6,36−41] Our results support the hypothesis that formation of dissolved Ni-thiol (and potentially Ni-carboxyl) complexes enriches the dissolved Ni pool in heavy ^{60}Ni; however, thiol concentrations vary widely (<0.1−300 nM) across aquatic systems.[27,28,42,43] In low-latitude ocean waters where Ni isotope fractionation[6,36,37] is observed but thiol concentrations are generally low,[43,44] future research should consider the potential role of other low-molecular-weight reduced S species, which accumulate at here at significant concentrations (>100 nM).[44]

Our results suggest that incorporation of Ni into metalloproteins (Figure 2) generally favors ^{60}Ni (Figure 1), with fractionation magnitude dependent on binding site configuration. Recent work suggests that variability in expressed metalloproteomes can strongly influence variability in observed isotope distributions in multicellular organisms.[45,46] Within plants, differential fractionation by S, N, and O ligands in metalloproteins has been invoked to explain observed distributions of zinc and cadmium isotopes, among other metals.[12] Our data suggest that Ni isotope fractionation in plants may be affected by differential fractionation by metalloprotein ligands. From roots to shoots, and within shoots, Ni isotope fractionations can vary from −0.47 to +0.85‰[2−4,47] depending on plant age and phenological stage.[3,47] This variability likely reflects changes in both metabolism (manifesting as varied metalloprotein expression) and demand (with kinetic effects, e.g., during uptake, driving a positive fractionation effect under some conditions).[12] Only two known Ni-proteins arise in plants; of these, urease is most common. Urease (Figure 2C) is activated upon quantitative insertion of a Ni atom from accessory protein UreG,[48] which binds Ni using two histidines and two cysteines at its primary binding site[49] (Figure 2D). In a simple model wherein UreG accesses a cytosolic Ni^{2+} pool, our results suggest a $\Delta^{60}Ni_{urease\text{-}free}$ value of roughly +0.58 ± 0.09‰. This value is in relatively good agreement with the upper end of the range in Ni isotope fractionations within plants.[12]

Our results provide the first experimental evidence that the most common biological ligands fractionate Ni, favoring heavy ^{60}Ni, and that these fractionations can manifest at higher levels of biocomplexity. Future work should consider the factors governing the expression of these effects, including intracellular Ni trafficking, competitive interactions among ligands and with other transition metals, and the relative expression of kinetic (e.g., diffusive transport through the membrane or desolvation of aqueous Ni^{2+} before ligand-binding) versus equilibrium isotope effects. Ni isotope systematics remains a new frontier and a greater mechanistic understanding of both kinetic and equilibrium drivers of fractionation will ultimately be needed to fully leverage Ni isotopes in closing the marine Ni budget,[13] studying plant physiology,[12] and tracking microbial processes.[7,9]

■ ASSOCIATED CONTENT

Data Availability Statement

All experimental data are available in the Supporting Information associated with this article.

Supporting Information

The Supporting Information is available free of charge at https://pubs.acs.org/doi/10.1021/acs.estlett.4c01060.

Details pertinent to experimental design (Text S1; Figure S1) and all reported results and calculations in tabular format (Tables S1−S6) (PDF)

■ AUTHOR INFORMATION

Corresponding Author

Corday R. Selden − *Department of Marine and Coastal Sciences, Rutgers University, New Brunswick, New Jersey 08901, United States; Department of Earth and Planetary Sciences, Rutgers University, Piscataway, New Jersey 08854, United States;* orcid.org/0000-0002-5721-3061; Email: crselden@marine.rutgers.edu

Authors

Kathrin Schilling − *Department of Environmental Health Sciences, Mailman School of Public Health, Columbia University, New York, New York 10032, United States*

Anirban Basu − *Department of Environmental Health Sciences, Mailman School of Public Health, Columbia University, New York, New York 10032, United States;* orcid.org/0000-0002-4905-9156

Jennifer Timm − *Department of Marine and Coastal Sciences, Rutgers University, New Brunswick, New Jersey 08901,*

https://doi.org/10.1021/acs.estlett.4c01060
Environ. Sci. Technol. Lett. 2025, 12, 283−288

United States; Center for Advanced Biotechnology and Medicine, Rutgers University, Piscataway, New Jersey 08854, United States; Present Address: Evotec, Princeton, NJ 08540, U.S.A.

Naomi Saunders − *Lamont-Doherty Earth Observatory, Columbia University, New York, New York 10964, United States;* Present Address: Department of Earth Sciences, Royal Holloway University of London, Egham TW20 0EX, U.K

Nathan Yee − *Department of Earth and Planetary Sciences, Rutgers University, Piscataway, New Jersey 08854, United States; Department of Environmental Sciences, Rutgers University, New Brunswick, New Jersey 08901, United States;* orcid.org/0000-0002-1023-5271

Complete contact information is available at: https://pubs.acs.org/10.1021/acs.estlett.4c01060

Notes

The authors declare no competing financial interest.

■ ACKNOWLEDGMENTS

We thank Vikas Nanda and Paul Falkowski for the use of their facilities in carrying out the peptide experiments, and for their support, encouragement, and feedback. We further thank Alex Halliday for use of his facilities and resources in the preparation of samples for Ni isotope analysis. The experimental work presented here was supported by NASA Exobiology Grant NNX16AK02G and NASA Astrobiology Grant 80NSSC18M0093, which were awarded to N.Y. Isotope analysis was supported by NIEHS Career Development Grant P30ES009089 and NIEHS Superfund Program Grant P42ES033719, which were awarded to K.S. C.R.S. also gratefully acknowledges the Rutgers Presidential Postdoctoral Fellowship Program for support while writing this article.

■ REFERENCES

(1) Elliott, T.; Steele, R. C. The Isotope Geochemistry of Ni. *Reviews in Mineralogy and Geochemistry* **2017**, *82* (1), 511−542.

(2) Deng, T.-H.-B.; Cloquet, C.; Tang, Y.-T.; Sterckeman, T.; Echevarria, G.; Estrade, N.; Morel, J.-L.; Qiu, R.-L. Nickel and Zinc Isotope Fractionation in Hyperaccumulating and Nonaccumulating Plants. *Environ. Sci. Technol.* **2014**, *48* (20), 11926−11933.

(3) Estrade, N.; Cloquet, C.; Echevarria, G.; Sterckeman, T.; Deng, T.; Tang, Y.; Morel, J.-L. Weathering and Vegetation Controls on Nickel Isotope Fractionation in Surface Ultramafic Environments (Albania). *Earth and Planetary Science Letters* **2015**, *423*, 24−35.

(4) Ratié, G.; Quantin, C.; De Freitas, A. M.; Echevarria, G.; Ponzevera, E.; Garnier, J. The Behavior of Nickel Isotopes at the Biogeochemical Interface between Ultramafic Soils and Ni Accumulator Species. *Journal of Geochemical Exploration* **2019**, *196*, 182−191.

(5) Zelano, I. O.; Cloquet, C.; Fraysse, F.; Dong, S.; Janot, N.; Echevarria, G.; Montargès-Pelletier, E. The Influence of Organic Complexation on Ni Isotopic Fractionation and Ni Recycling in the Upper Soil Layers. *Chem. Geol.* **2018**, *483*, 47−55.

(6) Lemaitre, N.; Du, J.; de Souza, G. F.; Archer, C.; Vance, D. The Essential Bioactive Role of Nickel in the Oceans: Evidence from Nickel Isotopes. *Earth and Planetary Science Letters* **2022**, *584*, 117513.

(7) Wang, T.-H.; Zhang, Q.; Hsieh, T.-T.; Henderson, G.; Rickaby, R. Isotopic Evidence for Nickel Limitation of Biological Productivity in the Ocean. *Preprint* **2023**, na.

(8) Bian, X.; Yang, S.; Raad, R. J.; Odendahl, C. E.; Lanning, N. T.; Sieber, M.; Huang, K.; Fitzsimmons, J. N.; Conway, T. M.; John, S. G. Distribution and Cycling of Nickel and Nickel Isotopes in the Pacific Ocean. *Geophys. Res. Lett.* **2024**, *51* (16), No. e2024GL111115.

(9) Cameron, V.; Vance, D.; Archer, C.; House, C. H. A Biomarker Based on the Stable Isotopes of Nickel. *Proc. Natl. Acad. Sci. U. S. A.* **2009**, *106* (27), 10944−10948.

(10) Bian, X.; Yang, S.-C.; Raad, R. J.; Odendahl, C. E.; Lanning, N. T.; Sieber, M.; Huang, K.-F.; Fitzsimmons, J. N.; Conway, T. M.; John, S. G. Distribution and Cycling of Nickel and Nickel Isotopes in the Pacific Ocean. *Geophys. Res. Lett.* **2024**, *51*, e2024gl11115.

(11) Bian, X.; Yang, S.-C.; Raad, R. J.; Seelen, E. A.; Duan, R.; Chen, Y.; Fu, F.; Hutchins, D. A.; John, S. G. *Nickel Isotope Fractionation during Uptake into Marine Phytoplankton*; Goldschmidt, 2024.

(12) Wiggenhauser, M.; Moore, R. E.; Wang, P.; Bienert, G. P.; Laursen, K. H.; Blotevogel, S. Stable Isotope Fractionation of Metals and Metalloids in Plants: A Review. *Frontiers in plant science* **2022**, *13*, 840941.

(13) Little, S. H.; Archer, C.; McManus, J.; Najorka, J.; Wegorzewski, A. V.; Vance, D. Towards Balancing the Oceanic Ni Budget. *Earth and Planetary Science Letters* **2020**, *547*, 116461.

(14) Andreini, C.; Cavallaro, G.; Lorenzini, S.; Rosato, A. MetalPDB: A Database of Metal Sites in Biological Macromolecular Structures. *Nucleic Acids Res.* **2012**, *41* (D1), D312−D319.

(15) Timm, J.; Pike, D. H.; Mancini, J. A.; Tyryshkin, A. M.; Poudel, S.; Siess, J. A.; Molinaro, P. M.; McCann, J. J.; Waldie, K. M.; Koder, R. L.; et al. Design of a Minimal Di-Nickel Hydrogenase Peptide. *Science Advances* **2023**, *9* (10), No. eabq1990.

(16) Pasternack, R. F.; Gibbs, E.; Cassatt, J. Complexation Kinetics of Leucine with Nickel (II), Cobalt (II), and Copper (II). *J. Phys. Chem.* **1969**, *73* (11), 3814−3819.

(17) Karpel, R. L.; Kustin, K.; Pasternack, R. F. Metal Complexation Kinetics of Serine. *Biochimica et Biophysica Acta (BBA)-General Subjects* **1969**, *177* (3), 434−441.

(18) Ryan, B. M.; Kirby, J. K.; Degryse, F.; Scheiderich, K.; McLaughlin, M. J. Copper Isotope Fractionation during Equilibration with Natural and Synthetic Ligands. *Environ. Sci. Technol.* **2014**, *48* (15), 8620−8626.

(19) Selden, C. R.; Schilling, K.; Godfrey, L.; Yee, N. Metal-Binding Amino Acid Ligands Commonly Found in Metalloproteins Differentially Fractionate Copper Isotopes. *Sci. Rep.* **2024**, *14* (1), 1902.

(20) Nasef, M. M.; Yahaya, A. H. Adsorption of Some Heavy Metal Ions from Aqueous Solutions on Nafion 117 Membrane. *Desalination* **2009**, *249* (2), 677−681.

(21) Gall, L.; Williams, H.; Siebert, C.; Halliday, A. Determination of Mass-Dependent Variations in Nickel Isotope Compositions Using Double Spiking and MC-ICPMS. *Journal of Analytical Atomic Spectrometry* **2012**, *27* (1), 137−145.

(22) Saunders, N. J.; Barling, J.; Harvey, J.; Halliday, A. N. Heterogeneous Nickel Isotopic Compositions in the Terrestrial Mantle-Part 1: Ultramafic Lithologies. *Geochim. Cosmochim. Acta* **2020**, *285*, 129−149.

(23) Saunders, N. J.; Barling, J.; Harvey, J.; Fitton, J. G.; Halliday, A. N. Heterogeneous Nickel Isotope Compositions of the Terrestrial Mantle-Part 2: Mafic Lithologies. *Geochim. Cosmochim. Acta* **2022**, *317*, 349−364.

(24) Siebert, C.; Nägler, T. F.; Kramers, J. D. Determination of Molybdenum Isotope Fractionation by Double-spike Multicollector Inductively Coupled Plasma Mass Spectrometry. *Geochemistry, Geophysics, Geosystems* **2001**, *2* (7), na.

(25) Fujii, T.; Moynier, F.; Dauphas, N.; Abe, M. Theoretical and Experimental Investigation of Nickel Isotopic Fractionation in Species Relevant to Modern and Ancient Oceans. *Geochim. Cosmochim. Acta* **2011**, *75* (2), 469−482.

(26) Fujii, T.; Moynier, F.; Blichert-Toft, J.; Albarède, F. Density Functional Theory Estimation of Isotope Fractionation of Fe, Ni, Cu, and Zn among Species Relevant to Geochemical and Biological Environments. *Geochim. Cosmochim. Acta* **2014**, *140*, 553−576.

(27) Dupont, C. L.; Moffett, J. W.; Bidigare, R. R.; Ahner, B. A. Distributions of Dissolved and Particulate Biogenic Thiols in the Subartic Pacific Ocean. *Deep Sea Research Part I: Oceanographic Research Papers* **2006**, *53* (12), 1961−1974.

(28) Al-Farawati, R.; Van Den Berg, C. M. Thiols in Coastal Waters of the Western North Sea and English Channel. *Environ. Sci. Technol.* **2001**, *35* (10), 1902−1911.
(29) Tang, D.; Hung, C.; Warnken, K. W.; Santschi, P. H. The Distribution of Biogenic Thiols in Surface Waters of Galveston Bay. *Limnology and Oceanography* **2000**, *45* (6), 1289−1297.
(30) Zhang, J.; Wang, F.; House, J. D.; Page, B. Thiols in Wetland Interstitial Waters and Their Role in Mercury and Methylmercury Speciation. *Limnology and Oceanography* **2004**, *49* (6), 2276−2286.
(31) Boiteau, R. M.; Till, C. P.; Ruacho, A.; Bundy, R. M.; Hawco, N. J.; McKenna, A. M.; Barbeau, K. A.; Bruland, K. W.; Saito, M. A.; Repeta, D. J. Structural Characterization of Natural Nickel and Copper Binding Ligands along the US GEOTRACES Eastern Pacific Zonal Transect. *Frontiers in Marine Science* **2016**, *3*, 243.
(32) Achterberg, E. P.; Van Den Berg, C. M. Chemical Speciation of Chromium and Nickel in the Western Mediterranean. *Deep Sea Research Part II: Topical Studies in Oceanography* **1997**, *44* (3−4), 693−720.
(33) Nimmo, M.; Van den Berg, C.; Brown, J. The Chemical Speciation of Dissolved Nickel, Copper, Vanadium and Iron in Liverpool Bay, Irish Sea. *Estuarine, Coastal and Shelf Science* **1989**, *29* (1), 57−74.
(34) Donat, J. R.; Lao, K. A.; Bruland, K. W. Speciation of Dissolved Copper and Nickel in South San Francisco Bay: A Multi-Method Approach. *Anal. Chim. Acta* **1994**, *284* (3), 547−571.
(35) Laglera, L. M.; van den Berg, C. M. Photochemical Oxidation of Thiols and Copper Complexing Ligands in Estuarine Waters. *Marine Chemistry* **2006**, *101* (1−2), 130−140.
(36) Yang, S.-C.; Kelly, R. L.; Bian, X.; Conway, T. M.; Huang, K.-F.; Ho, T.-Y.; Neibauer, J. A.; Keil, R. G.; Moffett, J. W.; John, S. G. Lack of Redox Cycling for Nickel in the Water Column of the Eastern Tropical North Pacific Oxygen Deficient Zone: Insight from Dissolved and Particulate Nickel Isotopes. *Geochim. Cosmochim. Acta* **2021**, *309*, 235−250.
(37) Yang, S.-C.; Hawco, N. J.; Pinedo-González, P.; Bian, X.; Huang, K.-F.; Zhang, R.; John, S. G. A New Purification Method for Ni and Cu Stable Isotopes in Seawater Provides Evidence for Widespread Ni Isotope Fractionation by Phytoplankton in the North Pacific. *Chem. Geol.* **2020**, *547*, 119662.
(38) Archer, C.; Vance, D.; Milne, A.; Lohan, M. C. The Oceanic Biogeochemistry of Nickel and Its Isotopes: New Data from the South Atlantic and the Southern Ocean Biogeochemical Divide. *Earth and Planetary Science Letters* **2020**, *535*, 116118.
(39) Takano, S.; Tanimizu, M.; Hirata, T.; Shin, K.-C.; Fukami, Y.; Suzuki, K.; Sohrin, Y. A Simple and Rapid Method for Isotopic Analysis of Nickel, Copper, and Zinc in Seawater Using Chelating Extraction and Anion Exchange. *Anal. Chim. Acta* **2017**, *967*, 1−11.
(40) Takano, S.; Liao, W.-H.; Ho, T.-Y.; Sohrin, Y. Isotopic Evolution of Dissolved Ni, Cu, and Zn along the Kuroshio through the East China Sea. *Marine Chemistry* **2022**, *243*, 104135.
(41) Wang, R.-M.; Archer, C.; Bowie, A. R.; Vance, D. Zinc and Nickel Isotopes in Seawater from the Indian Sector of the Southern Ocean: The Impact of Natural Iron Fertilization versus Southern Ocean Hydrography and Biogeochemistry. *Chem. Geol.* **2019**, *511*, 452−464.
(42) Dyrssen, D.; Haraldsson, C.; Westerlund, S.; Årén, K. Indication of Thiols in Black Sea Deep Water. *Marine Chemistry* **1985**, *17* (4), 323−327.
(43) Swarr, G. J.; Kading, T.; Lamborg, C. H.; Hammerschmidt, C. R.; Bowman, K. L. Dissolved Low-Molecular Weight Thiol Concentrations from the US GEOTRACES North Atlantic Ocean Zonal Transect. *Deep Sea Research Part I: Oceanographic Research Papers* **2016**, *116*, 77−87.
(44) Fourrier, P.; Dulaquais, G. Low-molecular-weight Reduced Sulfur Substances: A Major Component of Nonvolatile Dissolved Organic Sulfur in the Pacific Ocean. *Limnology and Oceanography Letters* **2024**, *9* (6), 735−744.
(45) Larner, F.; McLean, C. A.; Halliday, A. N.; Roberts, B. R. Copper Isotope Compositions of Superoxide Dismutase and Metallothionein from Post-Mortem Human Frontal Cortex. *Inorganics* **2019**, *7* (7), 86.
(46) Albarède, F.; Telouk, P.; Lamboux, A.; Jaouen, K.; Balter, V. Isotopic Evidence of Unaccounted for Fe and Cu Erythropoietic Pathways. *Metallomics* **2011**, *3* (9), 926−933.
(47) Zelano, I.; Cloquet, C.; van Der Ent, A.; Echevarria, G.; Gley, R.; Landrot, G.; Pollastri, S.; Fraysse, F.; Montargès-Pelletier, E. Coupling Nickel Chemical Speciation and Isotope Ratios to Decipher Nickel Dynamics in the Rinorea Cf. Bengalensis-Soil System in Malaysian Borneo. *Plant and Soil* **2020**, *454*, 225−243.
(48) Alfano, M.; Cavazza, C. Structure, Function, and Biosynthesis of Nickel-dependent Enzymes. *Protein Sci.* **2020**, *29* (5), 1071−1089.
(49) Fong, Y. H.; Wong, H. C.; Yuen, M. H.; Lau, P. H.; Chen, Y. W.; Wong, K.-B. Structure of UreG/UreF/UreH Complex Reveals How Urease Accessory Proteins Facilitate Maturation of Helicobacter Pylori Urease. *PLoS Biology* **2013**, *11* (10), No. e1001678.

https://doi.org/10.1021/acs.estlett.4c01060
Environ. Sci. Technol. Lett. 2025, 12, 283−288